ARCHIVES
of
FOUNDRY ENGINEERING

ISSN (2299-2944)
Volume 2024
Issue 3/2024

123 – 128

10.24425/afe.2024.151301

18/3

Published quarterly as the organ of the Foundry Commission of the Polish Academy of Sciences

Abrasive Wear Resistance of High-Entropy AlCoCuFeNi Alloy in SiC Mixture

K. Chrzan [a, b, *], B. Kalandyk [b], M. Grudzień-Rakoczy [a], Ł. Rakoczy [c], K. Cichocki [c]

[a] Łukasiewicz Research Network – Krakow Institute of Technology,
Centre of Materials and Manufacturing Research, Poland
[b] AGH University of Krakow, Faculty of Foundry Engineering, Poland
[c] AGH University of Krakow, Faculty of Metals Engineering and Industrial Computer Science, Poland
* Corresponding author. E-mail address: chrzan@agh.edu.pl

Received 17.05.2024; accepted in revised form 28.08.2024; available online 11.10.2024

Abstract

The results of tribological tests carried out on two novel high-entropy alloys (HEAs) from the AlCoCuFeNi group are described in this study. Research was carried out using a Miller machine (ASTM G75 standard) in an abrasive slurry environment, which contained SiC and water in a 1:1 ratio. The results obtained showed a higher rate of abrasive wear in the material designated as D3 (total weight loss in D3-1.6g compared to 1.1g in the D5 alloy), characterised by a homogeneous microstructure and hardness of 186 HV_5. The second dual phase alloy, designated D5, was characterised by a lower rate of abrasive wear. In this alloy, the appearance of the second phase precipitates, evenly distributed throughout the entire volume, with higher hardness (760 $HV_{0,01}$) and in a content of approximately 65% has led to a decrease in wear. The different wear resistances of the tested materials are due to differences in the hardness of the phases that constitute the microstructure of the tested alloys and the interaction of hard abrasive particles with the tested material. This has a direct impact on the plastic nature of the deformation in the upper layers of the samples. A characteristic system of linear grooves and protrusions, visible on surface profiles, was observed on the surfaces tested. Small local defects were also observed as a result of hammering and subsequent removal of hard SiC abrasive particles from the alloys tested or, in the case of the D5 alloy, additional removal of precipitates of the harder phase from the matrix.

Keywords: High-entropy alloys, Microstructure, Hardness, Wear resistance, Miller machine

1. Introduction

High-entropy alloys (HEAs) are a relatively new class of materials that have been under intensive development since 2004, when the first works on HEAs were published [1, 2]. An HEA alloy is the alloy in which the entropy of the configuration in the liquid state is greater than 1.5R (which is equivalent to 12.471 J/mol*K) [3]. Another definition of HEA is that it consists of at least five elements whose contents are in the range of 5-35 at %. [4]. Most high-entropy alloys currently studied meet both definitions, although there are examples of alloys that meet only one of the rules. Initially, research focused mainly on equiatomic compositions, where the atomic contents of all the elements that make up the alloy are equal [5]. However, HEA alloys with different contents of individual components are being investigated more and more frequently. The chemical composition can be optimised without producing many materials [6].

In high-entropy alloys four basic effects have a strong influence on their properties. These are:

- The effect of high-configuration entropy, which causes the system to strive for supersaturation. This facilitates the formation of a solid solution structure in multicomponent systems instead of a mixture of simple intermetallic compounds [7].
- The effect of significant distortion of the crystal lattice, which causes high internal lattice stresses (in the event of the formation of a solution/solid solution structure). This translates into the mechanical properties of such materials [8].
- The effect of slow diffusion, which is related to the presence of atoms with different radii in the solid solution. This makes diffusion much more limited [9].
- The cocktail effect, which is related to the influence of many factors on the final properties of the material [10].

Many high-entropy alloys that have been tested are known to exhibit unique properties that often exceed those of currently

utilised materials. It is widely acknowledged that alloys possessing the FCC (Face Centred Cubic) structure exhibit good impact strength and plasticity at room temperature. On the other hand, alloys with the BCC (Body Centred Cubic) structure tend to have good mechanical properties when exposed to high temperatures [11].

Alloys with an FCC structure, such as those of the FeMnCoCrC group, exhibit a tensile strength of approximately 1055 MPa after cold formation, while maintaining an elongation at break of 22.6% [12]. Another example of materials with an FCC structure is the FeCoCrNiMn group of alloys, which are strengthened by γ precipitates and have an ultimate tensile strength of approximately 900 MPa at 700°C [13], which makes them a competitive material for currently used nickel-based superalloys [14]. Several high-entropy alloys have been tested and found to have good resistance to abrasive wear. For example, alloys of the AlCoCrFeNiTi family exhibit excellent resistance to abrasive wear and also possess anticorrosion properties [15]. Another example is the high-entropy alloy from the FeCoCrNiW family, which has an FCC structure and was subjected to abrasive wear resistance tests. The presence of $(Ni,Co)_xTi$ phases in the structure significantly affects the properties of the material, leading to its high resistance to abrasive wear.

Firstov [16] has shown that precipitation-strengthened alloys with σ phase exhibit high resistance to abrasive wear. These materials can also be used as anti-wear or anti-corrosion coatings, which can help reduce the amount of expensive material required, such as high-entropy alloys [17]. Examples of coatings with high resistance to abrasive wear include high-entropy alloys from the $Al_xCoCrFeNiSi$ group [18, 19], which can be produced using atmospheric plasma spraying and laser remelting techniques. These alloys, which contain high Al content, crystallise in the FCC structure and have phases with the BCC and Cr_3Si structure, significantly increasing both hardness and resistance to abrasive wear. The objective of this study is to verify the abrasive wear properties of two model alloys from the AlCoCuFeNi group, designated as D3 and D5. Between both variants, there are visible large differences in mechanical properties and microstructure. These facts cause that the same differences can occur in functional properties such as abrasive wear resistance.

2. Materials and methods

In this study, high-entropy alloys melted in a laboratory induction electric furnace were used. Two alloys from the AlCoCuFeNi group were selected, and pure materials were used in the melting process. All elements had a minimum purity of 99.5%. The liquid alloy was poured into heated ceramic moulds (T = 900°C) to obtain ingots with dimensions of 70x75x24 mm. The chemical composition analysis was carried out by atomic absorption spectrometry using a Thermo Scientific SOLAAR M6 spectrometer (Table 1).

Table 1.
Chemical composition of the investigated high-entropy alloys designated D3 and D5

Alloy	Element content, at %				
	Al	Co	Cu	Fe	Ni
D3	10.71	24.32	7.50	29.04	28.43
D5	17.40	18.94	18.71	23.54	21.42

The samples were annealed at 1000°C in a Nabertherm furnace for 10 hours under argon protection and then cooled in air. Samples for microstructure characterisation were subjected to a standard metallographic preparation. They were ground on 100-2000 grit sandpaper and then polished with diamond suspensions of 3 μm and 1 μm. Before examinations, the samples were chemically etched using Adler's reagent, which is a solution of $FeCl_3$ $(NH_4)_2CuCl_4$ in HCl. Microstructure examinations of D3 and D5 alloys were carried out using a Leica MEF 4M light microscope. The surface fraction of phases detected in the D5 alloy was determined using an automatic LeicaQWin image analyzer. Subsequent observations were performed using a JEOL JSM 7100F scanning electron microscope equipped with an EDX detector (from Oxford Instruments). The backscattered detector was used for image the microstructure, while the accelerating voltage was equal to 20 kV.

The Vickers hardness (5 kgf) of the alloys was measured using a Struers Duaramin 40M1 hardness tester according to the ISO 6507-1:2023 standard [20]. In the case of sample D5, the microhardness of the phases present in the microstructure was also measured (0.1 kgf).

Wear resistance tests were performed using a Miller machine according to the ASTM G75 standard (Fig. 1) [21]. Samples for abrasion tests were taken from a 12 mm wall thickness casting. The device allows for the testing of four materials at the same time. Each sample with dimensions of 25.4x12.7x7 mm was moved to a separate trough containing an abrasive mixture of SiC (with a grain size of 53-73 μm) and H_2O (in a 1:1 ratio). The countersample was reinforced rubber placed at the bottom of each trough. During the 16-hour cycle, the samples underwent a reciprocating motion, each loaded with a force of 22.2 N. The samples were weighed every four hours on a balance with an accuracy of 0.001 g. Surface abrasion mark analysis was performed using a 3D LEXT TM OLS5100 confocal laser microscope from OPLYMPUS equipped with LEXT image analysis software.

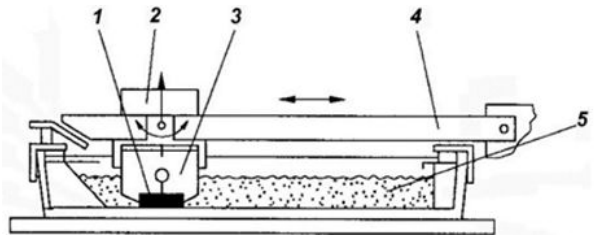

Fig. 1. Miller machine for wear resistance tests: 1- sample, 2- load, 3- holder for mounting the sample, 4 – runner, 5 – abrasive suspension

3. Results and Discussion

3.1. Microstructure and hardness

A typical dendritic microstructure with an irregular distribution of the phases characterises the microstructure of the D3 and D5 variants, which is visible in Figure 2. The microstructure of D3 is a relatively homogeneous single solid solution FCC system. Thus, only fine grey-contrasted precipitates are visible along grain boundaries. The microstructure of the D5 variant consists of light BCC and dark FCC phases (a detailed description of the results is available in another article prepared for publication). The surface fractions of the BCC phase and the FCC phase are 64.94 (± 3.6%)

and 35.06 (± 4.1%), respectively. Inside the FCC/BCC system, the fine strengthening precipitates (plate-like or blocky-shaped) precipitates are evenly distributed. Chemical composition analysis has revealed that the precipitates are characterised by a high concentration of Cu. Ren [22] observed precipitates similar to those in Fig. 3 in his research. These studies also indicate a high tendency to create two-phase structures with areas enriched in Cu (light precipitates in Fig. 4).

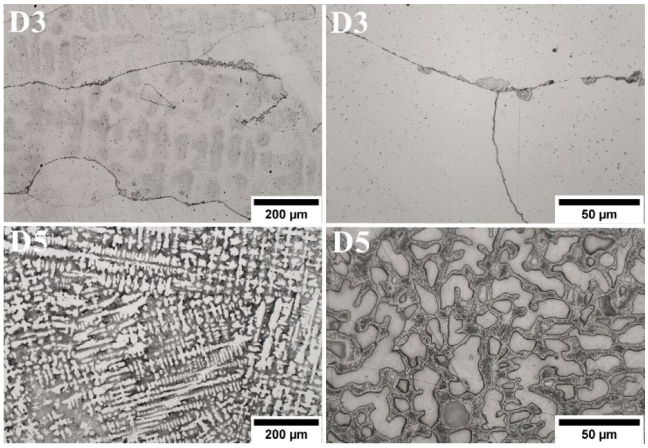

Fig. 2. Microstructure of high entropy alloys D3 and D5, LM

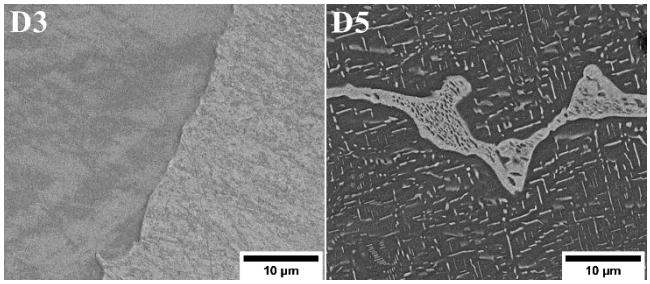

Fig. 3. Microstructure of high entropy alloys D3 and D5, SEM-BSE

When examining the chemical compositions of the light and dark areas in the D5 alloy, it becomes evident that the most prominent differences are in the concentration of Al and Cu (Table 2). Light precipitates contain more than twice the amount of Cu compared to the phase visible in the dark color. Additionally, a significant reduction in the amount of Al is observed in the light areas.

Table 2.
Results of the analysis chemical composition of selected areas of D3 and D5 alloys

Region/Element	Al	Co	Cu	Fe	Ni
D3 alloy					
FCC (at %)	7.8	28.6	5.4	29.8	29.9
Standard deviation	0.1	0.3	0.3	0.5	0.4
D5 alloy					
Dark phase - FCC (at %)	23.1	22.4	11.4	19.3	23.7
Standard deviation	0.2	0.5	1.0	0.2	0.5
Light phase - BCC (at %)	6.0	23.3	27.2	23.8	19.6
Standard deviation	0.2	0.1	0.3	0.1	0.2

When examining the chemical compositions of the light and dark areas (BSE phase contrast) in the D5 alloy, it becomes evident that the concentrations of Al and Cu are the most prominent differences. Light precipitates contain more than twice the amount of Cu compared to the phase visible in the dark color. Additionally, a significant reduction in Al content is observed in light areas.

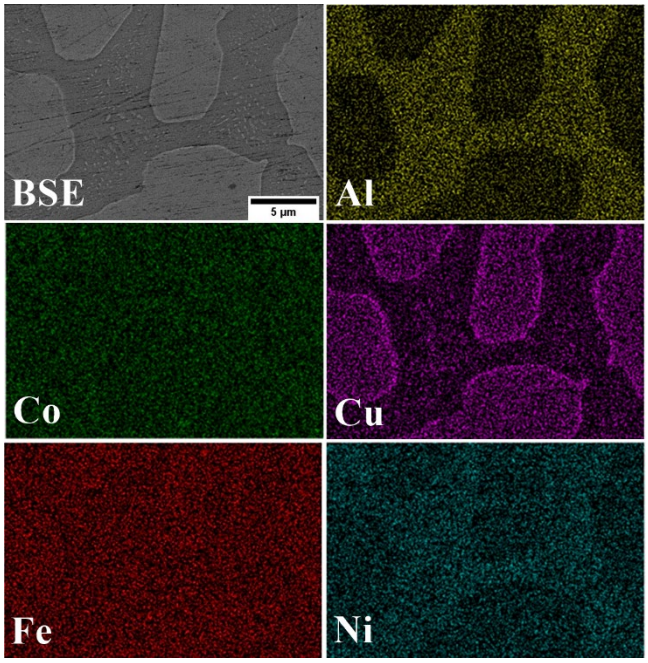

Fig. 4. Distribution maps of selected alloying elements, SEM-EDX

Due to differences in microstructure between D3 and D5, hardness tests were performed. The average hardness of the D3 alloy is equal to 186 HV_5 (± 8 HV_5), while in the case of D5 it is more than twice as high and amounts to 413 HV_5 (± 5 HV_5). It can be concluded that the presence of an additional phase with BCC structure has a strong influence on the increase in hardness. Due to the presence of fine precipitates within the solid FCC solution in D5 alloy, additional microhardness measurements were performed. A significant difference in hardness was found between the dark and light phases. The dark-colored phase had a hardness of 281 $HV_{0.01}$ (± 5 $HV_{0.01}$), while the phase visible in light color was characterised by a higher hardness of 761 $HV_{0.01}$ (± 8 $HV_{0.01}$). Large differences related to high concentration and distribution in structure could have a negative impact on brittleness and low plasticity.

3.2. Wear resistance test

Based on the results of the abrasion tests, it was found that the lowest total weight loss, amounting to 1.122 g, was obtained for the D5 alloy, while a much higher one, amounting to 1.646 g, was obtained for the D3 alloy (Fig. 5). Furthermore, a greater weight loss of the D5 alloy was observed after 8 and 16 hours, which could be caused by the chipping of small, hard precipitates present in its matrix. However, the weight loss of the D3 alloy after 8, 12 and 16 hours increases almost uniformly over time, which is related to its homogeneous microstructure and hardness.

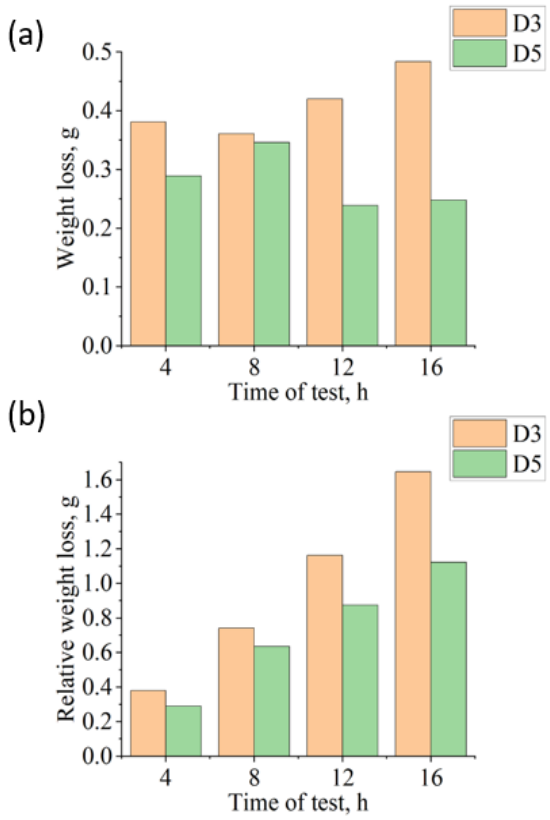

Fig. 5. Weight losses of the alloys D3 and D5 after wear test (a), Relative weight losses observed in the tested alloys (b)

During the tests, samples made of G20Mn5 cast steel and the high-entropy CoFeMnMoNi alloy were evaluated in parallel. Among the selected materials, the D3 and D5 alloys showed the highest wear. The D5 alloy showed a total weight loss similar to the G20Mn5 cast steel and the HEA CoFeMnMoNi alloy [23] (total wear rate: D3 - 1.646 g, D5 - 1.122 g, G20Mn5 - 0.993 g, CoFeMnMoNi - 0.973 g). This indicates that the low hardness of the D3 alloy significantly affects abrasive wear. However, in the case of the variant D5, it can be concluded that the precipitation of the second hard phase (the content of this phase in the microstructure is 35.06%) has a positive effect on the resistance to abrasive wear.

On the basis of the microstructural examinations carried out on the abraded surfaces of the tested alloys, it was found that they had undergone plastic deformation. This deformation was visible in all samples in the form of regular grooves and protrusions (Fig. 6). They were linear in nature, consistent with the direction of movement of the sample in the Miller test. Compared to sample D5, sample D3 had more densely arranged grooves on its surface, most probably due to its lower hardness and the impact of hard SiC particles present in the abrasive mixture (Fig. 6a,b). They can abrade the tested surfaces (causing the effect of microcuts) or stick into the soft matrix and then be torn out later of it.

In the case of the D5 alloy, the tests carried out revealed a linear arrangement of grooves and protrusions similar to that of D3, passing through the areas of two phases, light and dark, observed on the surface (Fig. 6c,d). SEM-EDS chemical composition analysis has shown an enrichment of the light phase, compared to the dark one, mainly in Cu and slightly in Co and Fe, with depletion in Al and Ni, which could have affected the wear rate of this alloy (Table 2). The images of the surface topography and respective profiles recorded with a confocal microscope are shown in Figure 7.

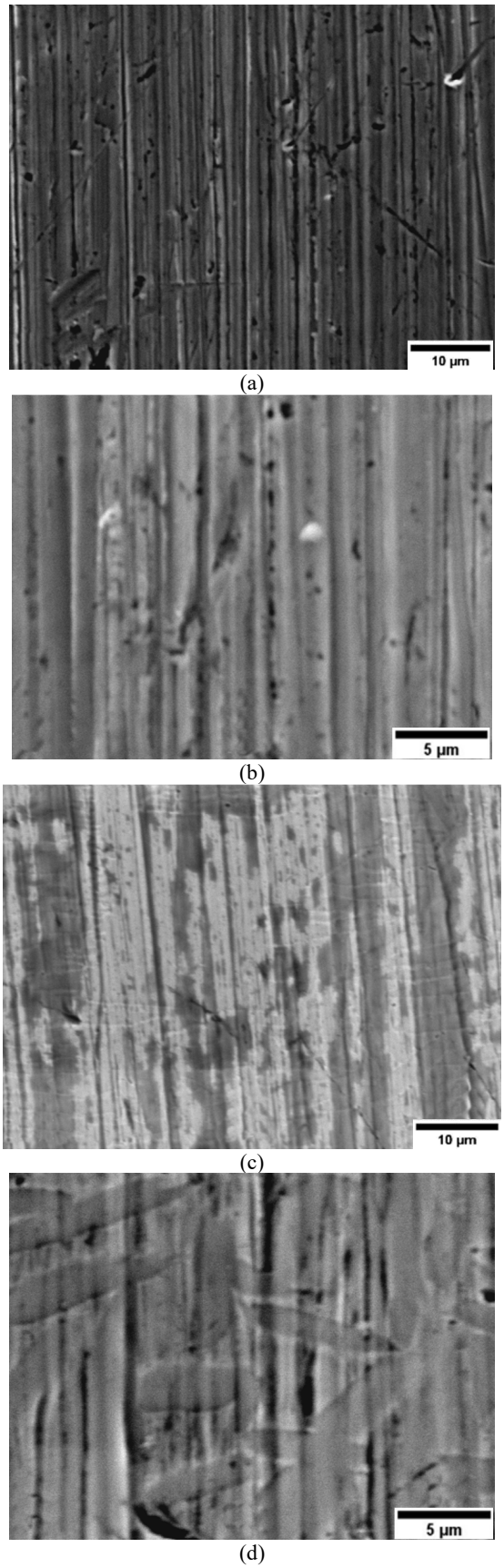

Fig. 6. SEM images of wear surfaces: (a-b) D3 alloy, (c-d) D5 alloy; scanning electron microscope

Based on the analysis of the profiles of worn surfaces recorded for the tested alloys, the influence of loose SiC particles contained in the abrasive mixture and the movement of samples in the Miller test on plastic deformation and the appearance of a system of grooves and protrusions on the tested surfaces was confirmed (Fig. 7).

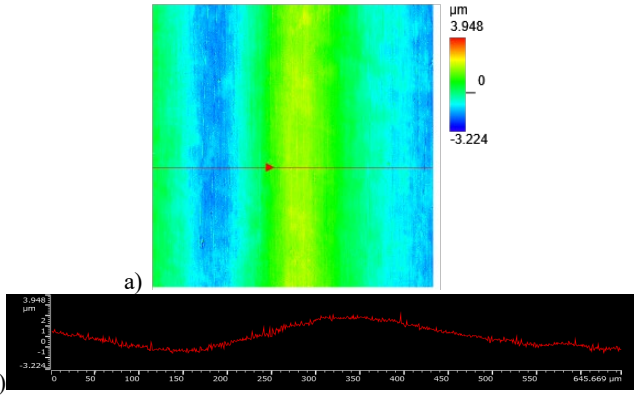

Fig. 7. 2D Surface profiles on cross-section (a) sample D3, (b) sample D5; confocal microscope

4. Conclusions

- The chemical composition, parameters of microstructure morphology (phase fraction) and hardness of the tested HEA alloys from the AlCoCuFeNi group have a significant impact on their resistance to abrasive wear. Compared to the D3 alloy, the chemical composition of the D5 alloy close to the equiatomic level offers much better resistance to abrasive wear in a mixture containing hard SiC particles. This is related to the higher hardness of the D5 alloy and its microstructure different from the microstructure of the tested alloy designated as D3. D5 alloy have similar properties, and microstructure like in other papers [24]
- Based on SEM examinations of surface topography after the test, it was found that in both tested alloys, directed plastic deformation had occurred in their surface layers and it was directly related to the type of tribosystem present in the pair involved in abrasive wear. The surface topography of both alloys was characterised by the presence of ridges, grooves, and scratches, all in a linear arrangement consistent with the direction of sample movement during the test. Additionally, point defects were observed to appear in microregions. They probably originated from the previously embedded and later pulled out hard abrasive particles or, in the case of the D5 alloy, small precipitates of a hard phase.
- The wear of the tested materials was accompanied by purely mechanical phenomena at the micro- and macroscopic level, and contrary to dry friction, the effect of tribooxidation did not occur. The dominant abrasion mechanism in this case was the interaction of loose SiC particles with the surface of the tested alloys.

The research was carried out as part of an implementation doctorate (project no. 68.10.170.07210).

References

[1] Cantor, B., Chang, I.T.H., Knight, P. & Vincent, A.J.B. (2004). Microstructural development in equiatomic multicomponent alloys. *Materials Science and Engineering: A*. 375-377, 213-218. https://doi.org/10.1016/j.msea.2003.10.257.

[2] Yeh, J.-W., Chen, S.-K., Lin, S.-J., Gan, J.-Y., Chin, T.-S., Shun, T., Tsau, C.-H., Chang, SY. (2004). Nanostructured high-entropy alloys with multiple principal elements: novel alloy design concepts and outcomes. *Advanced Engineering Materials*. 6. 299 - 303. https://doi.org/10.1002/adem.200300567.

[3] Dastur, Y.N. & Leslie, W.C. (1981). Mechanism of work hardening in Hadfield manganese steel. *Metallurgical Transactions A*. 12A, 749-759. https://doi.org/10.1007/BF02648339.

[4] Yeh, J.W. (2013). Alloy Design Strategies and Future Trends in High-Entropy Alloys. *JOM.* 65, 1759-1771. https://doi.org/10.1007/s11837-013-0761-6.

[5] Lu, Z.P., Wang, H., Chen, M.W., Baker, I., Yeh, J.W., Liu, C.T., Nieh, T.G. (2015). An assessment on the future development of high-entropy alloys: Summary from a recent workshop. *Intermetallics*. 66, 67-76, https://doi.org/10.1016/j.intermet.2015.06.021.

[6] Cichocki, K., Bała, P., Kozieł, T., Cios, G., Schell N. & Muszka, K. (2022). Effect of mo on phase stability and properties in FeMnNiCo high-entropy alloys. *Metallurgical and Materials Transactions A.* 53, 1749-1760 https://doi.org/10.1007/s11661-022-06629-x.

[7] Zhao, D.Q., Pan, S.P., Zhang, Y., Liaw, P.K. & Qiao, J.W. (2021) Structure prediction in high-entropy alloys with machine learning. *Applied Physics Letters*. 118(23), 231904. https://doi.org/10.1063/5.0051307.

[8] Yeh, J.W. (2015). Physical Metallurgy of high-entropy alloys. *JOM.* 67, 2254-2261. https://doi.org/10.1007/s11837-015-1583-5.

[9] Wang, R., Tang, Y., Li, S., Ai, Y., Li, Y., Xiao, B., Zhu, L., Liu, X. & Bai, S. (2020). Effect of lattice distortion on the diffusion behavior of high-entropy alloys. *Journal of Alloys and Compounds*. 825, 154099, 1-8. https://doi.org/10.1016/j.jallcom.2020.154099.

[10] Mehta, A. & Sohn, Y.H. (2021). Effects in transition metal high-entropy alloys: 'high-entropy' and 'sluggish diffusion' effects. *Diffusion Foundations*. 29, 75-93. https://doi.org/10.4028/www.scientific.net/DF.29.75.

[11] Cao, B.X., Wang, C., Yang, T., Liu, C.T. (2020) Cocktail effects in understanding the stability and properties of face-centered-cubic high-entropy alloys at ambient and cryogenic temperatures. *Scripta Materialia*. 187. 250-255. https://doi.org/10.1016/j.scriptamat.2020.06.008.

[12] Senkov, O.N., Wilks, G.B., Miracle, D.B., Chuang, C.P. & Liaw, P.K. (2010). Refractory high-entropy alloys. *Intermetallics*. 18(9), 1758-1765. https://doi.org/10.1016/j.intermet.2010.05.014.

[13] Varvenne, C., Luque, A. & Curtin, W.A. (2016) Theory of strengthening in fcc high entropy alloys. *Acta Materialia.* 118, 164-176. https://doi.org/10.1016/j.actamat.2016.07.040.

[14] Li, Z., Fu, L., Peng, J., Zheng, H., Ji, X., Sun, Y., Ma, S. & Shan, A. (2020). Improving mechanical properties of an FCC high-entropy alloy by γ′ and B2 precipitates strengthening, *Materials Characterization,* 159, 109989, 1-11. https://doi.org/10.1016/j.matchar.2019.109989.

[15] Chuang, M.H., Tsai, M.H., Wang, W.R., Lin, S.J. & Yeh, J.W. (2011). Microstructure and wear behavior of AlxCo1.5CrFeNi1.5Tiy high-entropy alloys. *Acta Materialia.* 59(16), 6308-6317. https://doi.org/10.1016/j.actamat.2011.06.041.
[16] Grudzień-Rakoczy, M., Rakoczy, Ł., Cygan, R., Chrzan, K., Milkovič, O. & Pirowski, Z. (2022). Influence of Al/Ti ratio and ta concentration on the As-cast microstructure, phase composition, and phase transformation temperatures of lost-wax Ni-based superalloy castings. *Materials.* 15(9), 3296, 1-26. https://doi.org/10.3390/ma15093296.
[17] Firstov, S.A., Gorban', V.F., Krapivka, N.A. Karpets, M.V. & Kostenko, A.D. (2017). Wear resistance of high-entropy alloys. *Powder Metallurgy and Metal Ceramics*. 56, 158-164. https://doi.org/10.1007/s11106-017-9882-8.
[18] Fan, Q., Chen, C., Fan, C., Liu, Z., Cai, X., Lin, S. & Yang, C. (2021). AlCoCrFeNi high-entropy alloy coatings prepared by gas tungsten arc cladding: Microstructure, mechanical and corrosion properties. *Intermetallics*. 138, 107337, 1-17. https://doi.org/10.1016/j.intermet.2021.107337.
[19] Yan, G., Zheng, M., Ye, Z., Gu, J., Li, C., Wu, C., Wang, B. (2021). In-situ Ti(C, N) reinforced AlCoCrFeNiSi-based high entropy alloy coating with functional gradient double-layer structure fabricated by laser cladding. *Journal of Alloys and Compounds.* 886, 161252, 1-8. https://doi.org/10.1016/j.jallcom.2021.161252.
[20] Standard- ISO 6507-1:2023- Metallic materials-Vickers hardness test.
[21] Standard- ASTM G75-15(2021)- Standard Test Method for Determination of Slurry Abrasivity (Miller Number) and Slurry Abrasion Response of Materials (SAR Number).
[22] Ren, Y., Wu, H., Liu, B., Liu, Y., Guo, S., Jiao, Z.B. & Baker, I. (2022). A comparative study on microstructure, nanomechanical and corrosion behaviors of AlCoCuFeNi high entropy alloys fabricated by selective laser melting and laser metal deposition. J*ournal of Materials Science & Technology.* 131, 221-230. https://doi.org/10.1016/j.jmst.2022.05.035.
[23] Cichocki, K., Bała, P., Kwiecień, M., Szymula, M., Chrzan, K., Hamilton, C. & Muszka, K. (2024). The influence of Mo addition on static recrystallization and grain growth behaviour in CoNiFeMn system subjected to prior deformation. *Archives of Civil and Mechanical Engineering.* 24. https://doi.org/10.1007/s43452-024-00888-8.
[24] Xiao, D.H., Zhou, P.F., Wu, W.Q., Diao, H.Y., Gao, M.C., Song, M. & Liwae, P.K. (2017). Microstructure, mechanical and corrosion behaviors of AlCoCuFeNi-(Cr,Ti) high entropy alloys. *Materials & Design.* 116, 438-447. https://doi.org/10.1016/j.matdes.2016.12.036.